Alternatively, rates can be inferred from induction times determined from shock tube measurements of ignition delay time τ. For pentane data, see Burcat and Dvinyaninov (1995), Burcat et al. (1971) and the more recent work of Bugler et al. (2016), A simple way to interpret induction time t_{ind} is as the characteristic decay time τ for fuel concentration

$$\frac{\mathrm{d}[\mathcal{F}]}{\mathrm{d}t} = \dot{\omega}_{\mathcal{F}} \,, \tag{10.134}$$

$$= -\frac{\mathcal{F}}{\tau} \,. \tag{10.135}$$

Given an empirical expression for t_{ind} as a function of temperature and reactant concentrations, the equivalent reaction rate is

$$k = \frac{[\mathcal{F}]}{t_{ind}} \,. \tag{10.136}$$

For example, Burcat and Dvinyaninov give the following correlation for induction time in pentane-oxygen mixtures diluted with Ar

$$t_{ind} = 10^{-12.8} \exp(+34610/\mathcal{R}T)[\mathrm{nC_5H_{12}}]^{0.29}[\mathrm{O_2}]^{-1.1}[\mathrm{Ar}]^{0.13} \,, \tag{10.137}$$

and the effective reaction rate is

$$k = 6.3 \times 10^{12} \exp(-34610/\mathcal{R}T)[\mathrm{nC_5H_{12}}]^{0.71}[\mathrm{O_2}]^{1.1}[\mathrm{Ar}]^{-0.13} \,. \tag{10.138}$$

Both the expressions of Westbrook and Dryer and Burcat and Dvinyaninov for the reaction rate are provided in pentane_one_step.cti and

Shock tube induction time data is most appropriate for validating reaction mechanisms for detonations. However, care is needed because induction time is measured in a variety of ways including pressure rise, heat flux, emission of electronically excited species or absorption using specific wavelengths or wavelength modulation. Different ways of measuring induction time must be accounted for in combining data sets and validating reaction models. There are also significant facility effects such as pressure changes during the induction time that need to be considered. A compendium of data (as of 2000) for hydrogen, ethylene and propane and discussion of instrumental and facility issues is given in Schultz and Shepherd (2000).[3] Shock tube induction time data are often the foundation (particularly at high temperature) in the development and validation of detailed chemical reaction models such as Bugler et al. (2016). Although common in past studies, these find limited use in calibrating one-step models, which are primarily used in analytical and computational studies that seek insights into the interaction between fluid mechanics and chemical reactions in multi-dimensional transient flows for which detailed reaction mechanisms are not practical for doing extensive parametric studies. More realistic than one-step reactions are multi-step models Liang et al. (2007) which have some of the features that mimic aspects of detailed models without the computational overhead.

In Fig. 10.12, the computed temperature histories are shown for a detailed reaction model of pentane-combustion and compared to two one-step models. The predictions of the detailed model are substantially different than either one-step model. The detailed model predicts that the initial temperature drops due to endothermic reactions associated with the breakdown of the fuel to smaller hydrocarbons and there is a very sharp temperature rise at the end of the induction period. In contrast, the one-step models are entirely exothermic, do not have a clearly defined induction period or a distinct energy release transient. The one-step models also predict a much faster reaction rate than the detailed model. In part, this is due to the very different regimes of pressure and concentration as well as the types of combustion data used for validation in the case of Westbrook and Dryer (1981). Experiments in air at pressures up to 2 MPa are reported in Bugler et al. (2016) but the induction times are given in terms of OH^* emission peaks rather than pressure rise so careful interpretation with a detailed reaction mechanism (including OH^* production and destruction) is required in order to use this data for validation.

[3]The validation results presented in this report are for older reaction mechanisms without proper models for excited species. However, the tabulation of experimental data obtained by digitizing plots is still quite useful.

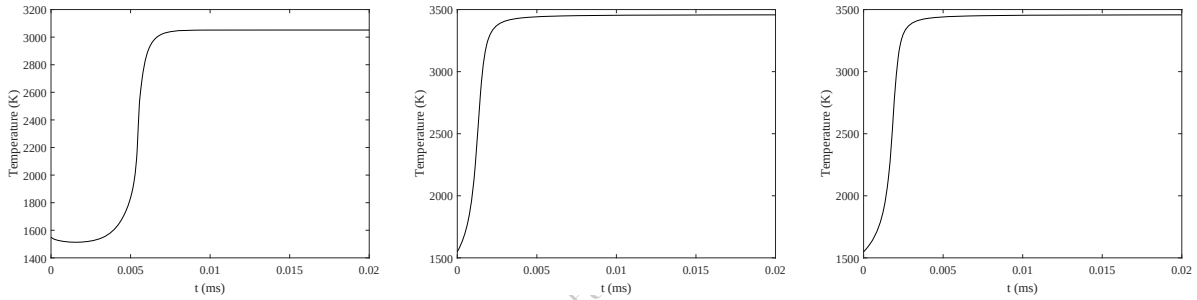

Figure 10.12: Example constant-pressure combustion simulation with three reaction and thermodynamic models, same initial conditions as in Fig. 10.11. a) Detailed chemistry and thermodynamics using the JetSurf2 mechanism. b) One-step reaction of Westbrook and Dryer (1981) c) One-step reaction of Burcat and Dvinyaninov (1995).

Chapter 11

Applications

The formulation of the reaction zone equations and applications to steady and unsteady flows, was introduced in Ch. 10. In this chapter, reaction zones behind propagating and stationary shock or detonation waves are considered for a variety of applications. This includes the standard ZND model for detonations, zero-dimensional models with prescribed pressure and volume changes, propagating waves with curvature, steady and moving waves in ducts with friction and heat interactions, the shock change equation, stagnation point flows and the effects of vibrational-translational nonequilibrium behind shock waves.

11.1 Steady shock waves followed by reaction zones

The reaction zone behind a planar shock moving with a constant speed can for many purposes be analyzed in a shock-fixed reference frame as an inviscid, adiabatic flow. Under these conditions the flow properties will satisfy the conservation relations for steady one-dimensional compressible flow at each point.

$$\rho \mathrm{w} = \rho_1 \mathrm{w}_1 \tag{11.1}$$

$$P + \rho \mathrm{w}^2 = P_1 + \rho_1 \mathrm{w}_1^2 \tag{11.2}$$

$$h + \frac{1}{2}\mathrm{w}^2 = h_1 + \frac{1}{2}\mathrm{w}_1^2 \tag{11.3}$$

and evolves due to the change in chemical composition with distance downstream from the shock.

$$w\frac{\mathrm{d}Y_k}{\mathrm{d}x} = \frac{\mathcal{W}_k \dot{\omega}_k}{\rho} \qquad (k = 1, \ldots, K) \tag{11.4}$$

Following a parcel of gas downstream from the shock the distance traveled and time elapsed are related by integrating in time to find distance x along the stream line

$$\frac{\mathrm{d}x}{\mathrm{d}t} = \mathrm{w} \; . \tag{11.5}$$

The formulation given above is equivalent to the steady flow reaction model developed previously in Ch. 9.6 which can be expressed in terms of spatial derivatives as

$$w\frac{\mathrm{d}\rho}{\mathrm{d}x} = -\rho\frac{\dot{\sigma}}{\eta} \; , \tag{11.6}$$

$$w\frac{\mathrm{d}P}{\mathrm{d}x} = -\rho w^2\frac{\dot{\sigma}}{\eta} \; , \tag{11.7}$$

$$w\frac{\mathrm{d}w}{\mathrm{d}x} = w\frac{\dot{\sigma}}{\eta} \; , \tag{11.8}$$

$$w\frac{\mathrm{d}Y_k}{\mathrm{d}x} = \frac{1}{\rho}\mathcal{W}_k\dot{\omega}_k = \Omega_k \qquad (k = 1, \ldots, K) \; . \tag{11.9}$$

The solution to these equations for both shock and detonation waves is implemented in the ZND solvers discussed below.

Considering the reaction zone structure computation downstream of a shock as an initial value problem, state 1 is the condition immediately behind the shock wave ($t = 0$ or $x = 0$) as determined by the solution to the (frozen) shock jump conditions. The equations are valid for both endothermic and exothermic reaction zones.

Endothermic Reactions

Endothermic reaction zones occur behind shock waves in high-speed atmospheric flight and planetary reentry as well as laboratory testing in shocks or related high-speed flow facilities. These endothermic processes may include exchange of energy between translation, rotation and vibration can also be included in a steady flow framework but require extensions of the thermodynamic model and reaction mechanisms that we defer to later discussion.

For endothermic flows there is no limitation on the shock speed unlike the case of exothermic flows (detonations) that is discussed next. Solutions for the reaction behind a strong shock in air are shown in Fig. 11.1.

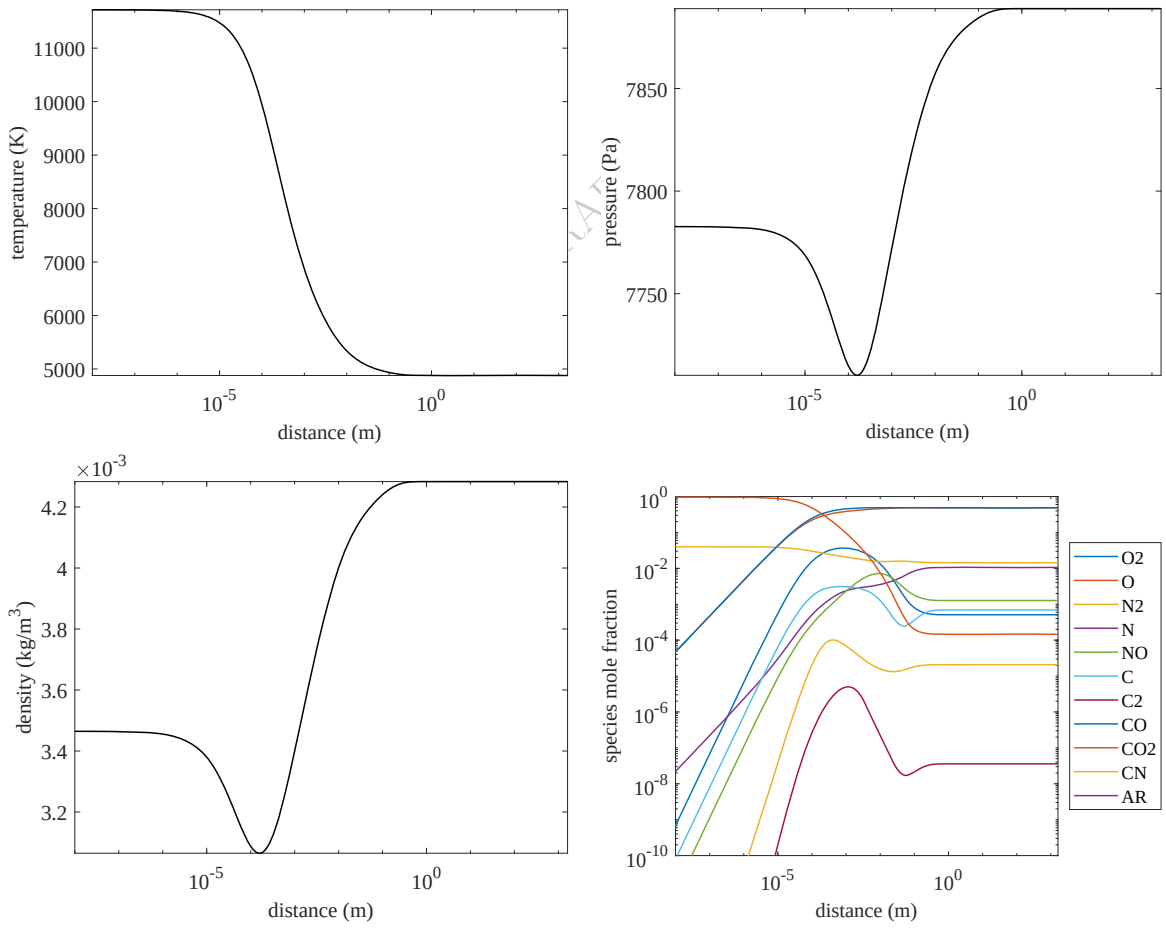

Figure 11.1: Reaction zone structure behind a strong shock wave ($U = 6000$ m/s) in a mixture of N_2/CO_2 (4/96) initially at 13.3 Pa and 300 K.

11.2 ZND Detonation Model

The ZND detonation model is a one-dimensional steady model, which can be expressed by an algebraic-differential system of equations or a purely differential system of equations. First we will discuss physical and graphical interpretations of this model.

Physical Model

A detonation is a supersonic combustion wave in which a shock wave and a reaction zone are coupled. The leading shock raises the temperature and pressure of a mixture of fuel and oxidizer initiating a coupled thermal branching-chain explosion. After an induction time, exothermic recombination reactions create product species whose expansion acts as a piston propelling the shock wave forward. The interaction between the leading shock and consequent reaction zone is a defining characteristic of self-sustained detonations.

The simplest detonation model, the ZND model, was developed in the 1940s independently by Zel'dovich (1940), von Neumann (1942), and Doering (1943). In this model, shown in the wave-fixed frame in Fig. 11.2, a frozen shock is followed by a finite reaction zone. State 1 is a cold mixture of reactants, state 2 is a shocked (hot) mixture of the same reactants, and state 3 is the equilibrium state of the reactive mixture. This model assumes that the composition does not change between states 1 and 2. Within the reaction zone, there are two main length scales: Δ_i, the induction length, and Δ_e, the energy release pulse width. These two scales will be discussed further in relation to the mathematical model. The equations presented in the steady-state model approximate the path between states 2 and 3.

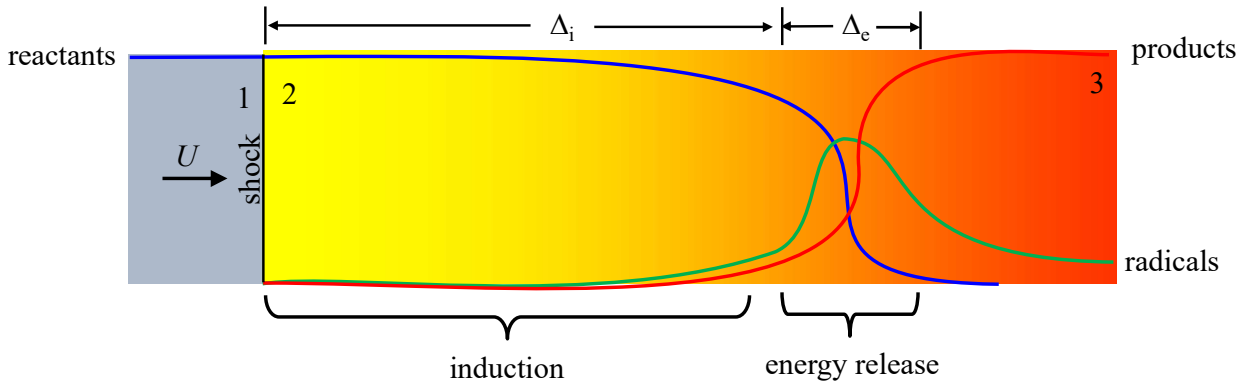

Figure 11.2: Schematic of the ZND detonation model. (a) States 1, 2, and 3 (b) Reaction zone structure.

Figure 11.3 illustrates how we can visualize this model in the P-v plane with the Rayleigh line (Eq. B.4) and Hugoniot curve (Eq. B.5). A frozen shock wave connects states 1 and 2. We see that in this figure, the Rayleigh line is tangent to the product Hugoniot which indicates that this is the CJ case. State 2, the frozen post-shock state, for the CJ case is often called the von Neumann (vN) point. For an overdriven detonation, state 2 is simply the frozen post-shock state. State 3 lies on the same Rayleigh line, but on the equilibrium Hugoniot rather than the frozen Hugoniot. We see that in the ZND model, both the pressure and the specific volume vary through the reaction zone. In reactive systems, there are many Hugoniot curves for each amount of partial reaction ranging from frozen to total equilibrium. Although only the frozen and equilibrium Hugoniots are shown in Fig. 11.3 each point along the red line connecting states 2 and 3 lies on a partial equilibrium Hugoniot.

ZND Software

The ZND model and variations are implemented in the SDToolBox. Simple examples of how to use these functions are given in the following demonstration programs.

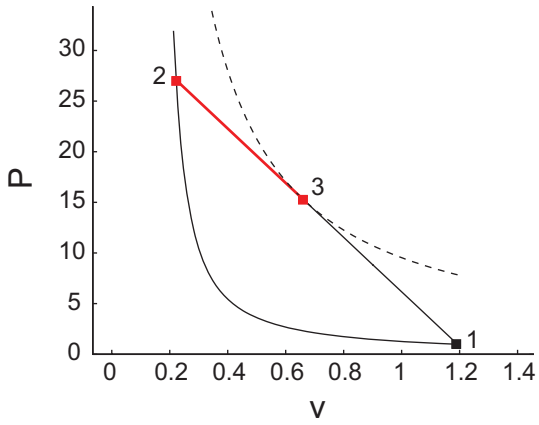

Figure 11.3: Path (red) between frozen Hugoniot (solid) and equilibrium Hugoniot (dashed) for a ZND detonation traveling at the Chapman-Jouget detonation velocity.

- demo_ZNDCJ.py demo_ZNDCJ.m Solves ODEs for ZND model of detonation structure. Generate plots and output files for a for a shock front traveling at the CJ speed.
- demo_ZND.m Solves ODEs for ZND model of detonation structure. Generate plots and output files for a for a shock front traveling at the CJ speed. Provide reaction characteristics in terms of thermicity peak and half-width time and distance.
- demo_ZNDshk.py demo_ZNDshk.m Solves ODEs for ZND model of detonation structure. Generate plots and output files for a for a shock front traveling at a user specified speed U.
- The MATLAB programs implement the ordinary differential equation set in the functions zndsolve.m and zndsys.m.
- The Python programs implement the ordinary differential equation set in the class ZNDsys and module zndsolve.py.

An example of the ZND reaction zone structure for two examples are given in Figs. 11.4 and 11.5. A CJ detonation stoichiometric CH_4-air mixture at atmospheric pressure is shown in Fig. 11.4 and a highly-diluted stoichiometric H_2-O_2-Ar mixture at low pressure is shown in Fig. 11.5. These two mixtures represent extremes in structure for atmospheric pressure hydrocarbon-air and low-pressure highly-diluted mixtures typical of laboratory experiments as discussed further below.

Thermicity in ZND models

As discussed in Section 9.3, the coupling between the flow and the chemistry is represented by the thermicity (9.32), for an ideal gas a convenient form is

$$\dot{\sigma} = \sum_{k=1}^{K} \left(\frac{\mathcal{W}}{\mathcal{W}_k} - \frac{h_k}{c_p T} \right) \frac{\mathrm{D}Y_k}{\mathrm{D}t} \,.$$

The variation of the thermicity within the flow reflects the net effect and history of all chemical reactions taking place: bimolecular exchanges, recombination and dissociation. The magnitude and sign of $\dot{\sigma}$ depends on the rate at which each process is occuring, the net amount of energy released or absorbed, and the net creation or destruction of molecules.

The first term in (9.32) is the effective energy release associated with changing the total number of moles of species per unit mass of the reacting mixture. The second term in (9.32) is the normalized energy release associated with chemical bond breaking and formation. Normally, the second term completely dominates the

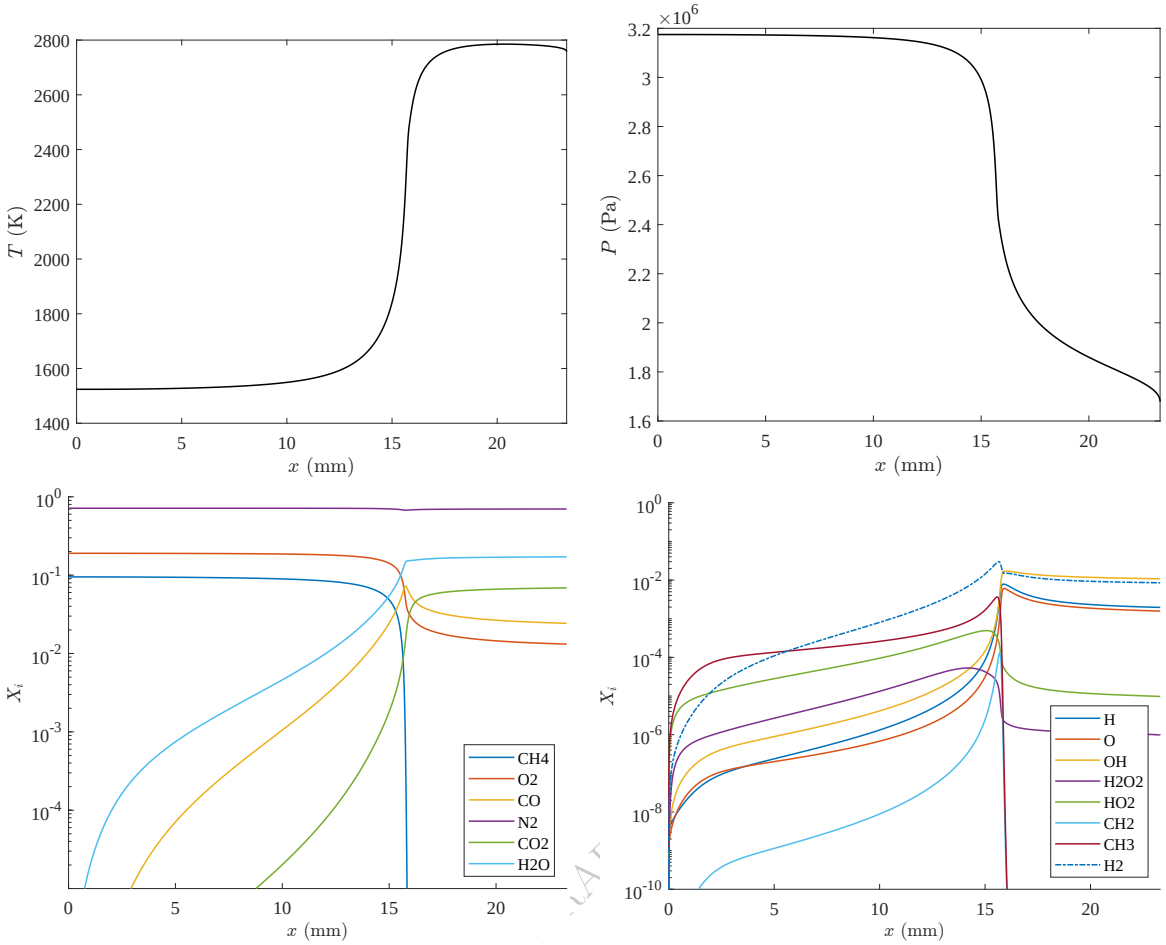

Figure 11.4: Reaction zone spatial profiles for the ZND model of a steady CJ detonation in a stoichiometric CH_4-air mixture with initial conditions of 25°C and 1 atm.

first. In those cases, if the dominant processes are endothermic reactions, $\dot{\sigma} < 0$; if the dominant processes are exothermic reactions, $\dot{\sigma} > 0$.

In general, thermicity is a dynamic property and evaluation can only be carried as part of simulation of a reacting flow. Thermicity in the steady ZND reaction zone behind a CJ detonation wave is often used to define the characteristic length and time scales. Examples of the thermicity spatial profiles in given in for two examples shown Fig. 11.4 and 11.5.

There are two key features of detonation reaction zones illustrated in these examples: a) there is dwell or induction time t_i (or induction distance Δ_i) during which very little energy is released or absorbed; b) there is an energy release event that occurs over a characteristic time t_e (or distance Δ_e). The relevance of these time scales is in comparison to the time scale of other flow processes such as flow pressure and temperature variation due to wave diffraction or area change, acoustic wave propagation time and instability period. The simplest notion used in analyzing detonations is that the induction time (or length) provides the fundamental scale that determines the other critical time (or length) scales in the problem. While only approximately true, this provides one of the key links between the chemical processes and the macroscopic wave behavior. The ratio t_i/t_e (or Δ_i/Δ_e) is highly correlated with the experimentally observed in stability characteristics of propagating detonations Ng et al. (2005) as is the effective activation energy Austin et al. (2005).

Various definitions of the induction and energy release times have been used by different researchers. Some researchers do not distinguish between these measures and simply report a "reaction zone" length Δ. While

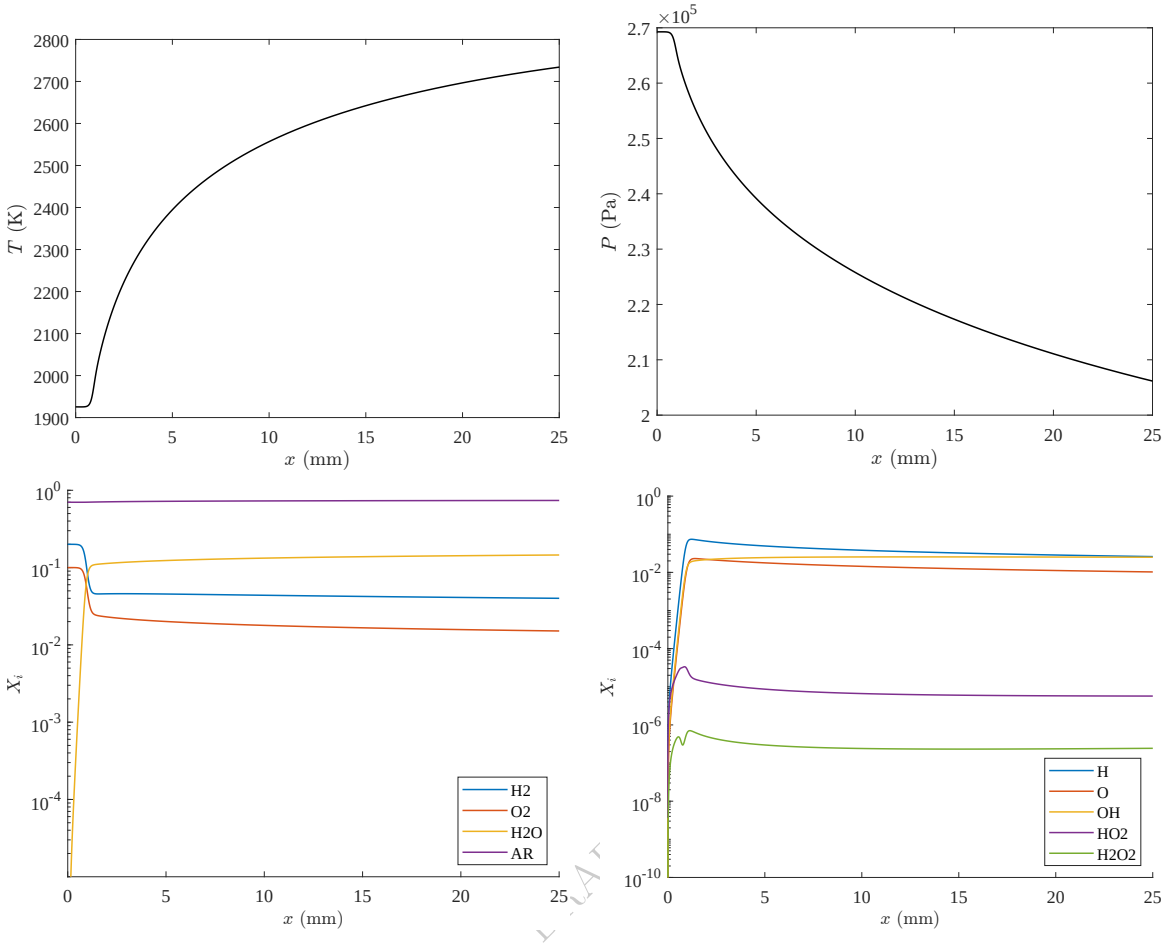

Figure 11.5: Reaction zone spatial profiles for the ZND model of a steady CJ detonation in a stoichiometric H_2-O_2-Ar mixture (70% Ar dilution) with initial conditions of 25°Cand 0.1 atm.

useful as a notion when carrying out order-of-magnitude computations or scaling terms in mathematical analyses, this is problematic when attempting to quantify reaction structure or determine the relationship to other detonation properties such as detonation cell width, critical tube or channel widths or initiation energy. Numerical solutions of the ZND model with a range of fuel-oxidizer-diluent mixtures reveal that there is a continuum of reaction zone structures ranging from systems without a distinct induction zone where $\Delta_i \approx \Delta_e$ to those with a very distinct and long induction zone in comparison with the energy release zone $\Delta_i \gg \Delta_e$ (see the discussion in Shepherd, 2009). In the example of Fig. 11.4, the thermicity peak can be used to define an induction length $\Delta_i = 16$ mm that is two orders of magnitude larger than the energy release length $\Delta_e = 0.25$ mm. On the other hand, in the example of Fig. 11.5, the thermicity peak $\Delta_i = 0.96$ mm an order of magnitude smaller than the energy release length $\Delta_e = 8.7$ mm.

The meaning of induction time is particular to the situation being described and may be various defined by spectroscopic emission or absorption peaks of certain species, arbitrary concentration, presssure or temperature rises. The concept of induction time or distance is often quantified by defining the induction time or distance in terms of the location where a certain property like temperature, pressure, or species concentrations increases by a small amount over the initial post-shock value, see the discussion in Akbar et al. (1997), Schultz and Shepherd (2000). A less arbitrary method that works well for systems with distinct induction periods and short energy release period is to define the end of the induction period by the location of the maximum rate of temperature or pressure rise.

A maximum temperature gradient or rate of change definition is convenient particularly for constant pressure or volume models of reaction processes, which have been used by some researchers as an approxi-

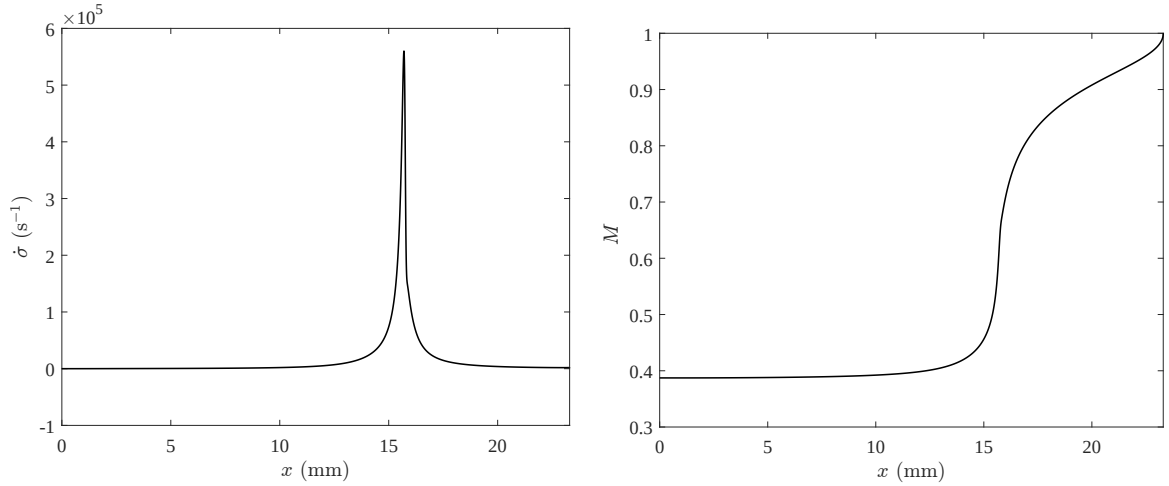

Figure 11.6: ZNd model results for (a) thermicity and (b) Mach number spatial profiles for the stoichiometric CH_4-air case shown in Fig. 11.4.

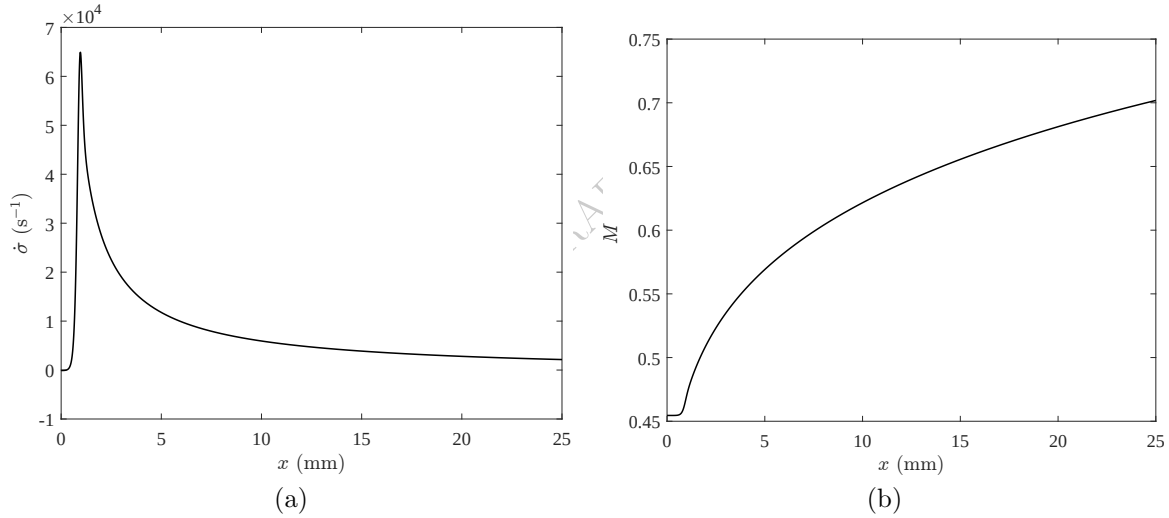

Figure 11.7: ZND model results for (a) thermicity and (b) Mach number spatial profiles for a steady CJ detonation for the stoichiometric H_2-O_2-Ar case shown in Fig. 11.5.

mation to the ZND model. For example, these models are often used to make estimates of ZND induction time and length by using the maximum temperature rate of change with time to define an induction time t_i. The induction zone length is then approximated by assuming a constant postshock velocity w_2 (evaluated at the vN point) and setting $\Delta_i = w_2 t_i$. Often, only a estimate of the reaction zone size is needed and such an approximate model of the reaction zone suffices. However, if the ZND model structure of the reaction zone is desired, particularly the details of the energy release zone, then it is necessary to compute the reaction progress along the Rayleigh line, which is equivalent to the numerical solution of (11.6 - 11.9).

Various methods have been proposed for characterizing reaction zone length scales, some preliminary efforts are discussed in Shepherd (1986). The most useful and unambiguous way to define the induction time (distance) for ZND simulations of detonations is by location of the thermicity maximum

$$t_i = t(\dot{\sigma}_{max}) \,, \quad \Delta_i = x(\dot{\sigma}_{max}) \,,$$

shown in Fig. 11.8. Time and distance are measured in the shock-fixed reference frame with the zero datum at the location of the shock front. The energy release time (distance) for detonations can be characterized by the width of the thermicity pulse. The width can be measured in various ways, one way is to find the duration (or distance) between the locations of an arbitrary fraction α of $\dot{\sigma}_{max}$ on the rising and falling portions of the thermicity.

$$t_e = t_{\dot{\sigma}_\alpha} = t\left(\dot{\sigma} = \alpha\dot{\sigma}_{max}, \frac{\mathrm{d}\dot{\sigma}}{\mathrm{d}t} < 0\right) - t\left(\dot{\sigma} = \alpha\dot{\sigma}_{max}, \frac{\mathrm{d}\dot{\sigma}}{\mathrm{d}t} > 0\right) , \tag{11.10}$$

or length

$$\Delta_e = \Delta_{\dot{\sigma}_\alpha} = x\left(\dot{\sigma} = \alpha\dot{\sigma}_{max}, \frac{\mathrm{d}\dot{\sigma}}{\mathrm{d}x} < 0\right) - x\left(\dot{\sigma} = \alpha\dot{\sigma}_{max}, \frac{\mathrm{d}\dot{\sigma}}{\mathrm{d}x} > 0\right) . \tag{11.11}$$

Lengths defined by fractions $\alpha = 0.5$ and 0.1 are defined in Fig. 11.8 and the value of 0.5 is reported by default in the programs demo_ZND.m and demo_ZNDshk.py.

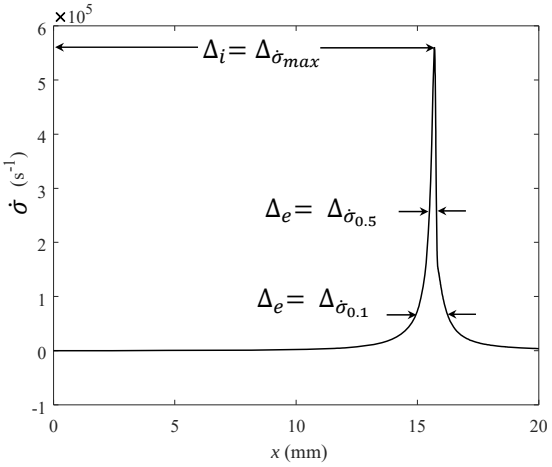

Figure 11.8: Definitions of induction and energy length based on thermicity profile for case shown in Fig. 11.4.

The CH_4-air detonation shown in Figs. 11.4 and 11.6 has a value of $\Delta_{\dot{\sigma}_{max}}/\Delta_{\dot{\sigma}_{0.1}} = 59$ whereas the stoichiometric H_2-O_2mixture diluted with 70% Ar shown in Figs.11.5 and 11.7 has value of $\Delta_{\dot{\sigma}_{max}}/\Delta_{\dot{\sigma}_{0.1}} = 1.7$. The CH_4-air detonation is observed to have highly irregular cellular structure whereas the Ar-diluted H_2-O_2mixture displays the classical regular cellular pattern (Austin et al., 2005).

Ng et al. (2005) defined the induction zone length based on the thermicity peak $\Delta_I = \Delta_{\dot{\sigma}_{max}}$ but used an alternative definition of energy release zone length $\Delta_R = w_2/\dot{\sigma}_{max}$. With these definitions, they propose a stability parameter

$$\chi = \Theta\frac{\Delta_I}{\Delta_R}$$

where Θ is the reduced effective activation energy $E_a/\mathcal{R}T_{\mathrm{vN}}$ computed on the basis of constant volume explosion computations. The length Δ_R is similar to the length Δ_e defined by the width of the thermicity function but not identical.

An unambiguous way to define the width or duration of the thermicity pulse is to define length or time scales using the integral of the $\dot{\sigma}$ temporal profile. One possibility is to define a characteristic pulse duration as

$$t_{\dot{\sigma}_p} = \frac{1}{\dot{\sigma}_{max}}\int_0^\infty \dot{\sigma}(t)\,\mathrm{d}t\,. \tag{11.12}$$

The integral can be estimated with the aid of the reaction zone structure equation (9.83)

$$\int_0^\infty \dot{\sigma}\,\mathrm{d}t = \int_{w_2}^{w_3} \frac{\eta}{w}\,\mathrm{d}w\,. \tag{11.13}$$

Inspection of the integrand on the righthand side indicates that it will be on the order of $\eta_{max}\ln(w_3/w_2)$. Using typical values of the velocities and sonic parameters, we find that this can be approximated as a constant C which has a value betweeen 0.4 and 0.7. We conclude that the pulse width can be well approximated as

$$t_{\dot{\sigma}_p} = \frac{C}{\dot{\sigma}_{max}} \propto \frac{1}{\dot{\sigma}_{max}} \tag{11.14}$$

In order to estimate the spatial extent of the pulse we have to transform to spatial coordinates and define a pulse width as

$$\Delta_{\dot{\sigma}_p} = \left(\frac{w}{\dot{\sigma}}\right)_{max} \int_0^\infty \frac{\dot{\sigma}(x)}{w(x)}\,\mathrm{d}x\,. \tag{11.15}$$

The integral is identical to what we have previously computed

$$\int_0^\infty \frac{\dot{\sigma}(x)}{w(x)}\,\mathrm{d}x = \int_0^\infty \dot{\sigma}(t)\,\mathrm{d}t = C \tag{11.16}$$

and we obtain the estimate

$$\Delta_{\dot{\sigma}_p} = C\frac{w_{max}}{\dot{\sigma}_{max}} \tag{11.17}$$

The relationship to Δ_R defined by Ng et al. can be obtained by approximating the velocity $w_{max} = w_2$ to obtain

$$\Delta_R = \frac{w_2}{\dot{\sigma}_{max}} \approx \Delta_{\dot{\sigma}_p}\,. \tag{11.18}$$

Values of the various reaction zone lengths are given in Table 11.1 for the CH_4-air and the H_2-O_2-Ar example.

A different measure of reaction zone length is used in analytical studies with idealized reaction models. A widely-used model is the one-step irreversible reaction $\mathcal{A} \rightarrow \mathcal{B}$ with constant ratio of specific heats and specified energy release. A standard method of characterizing the reaction zone is to normalize the length and time scales by the values at the point where one-half of the reactants $\mathcal{A}$ have been consumed, $\Delta_{1/2} = x(Y_\mathcal{A} = 0.5)$. The length or time scales $\Delta_{1/2}$ or $t_{1/2}$ can be related to thermicity measures $\Delta_{\dot{\sigma}_{max}}$ and $t_{\dot{\sigma}_{max}}$ but are not identical. For example, numerical simulation of the case $\Delta S = 0$ from Kao (2008) yields $\Delta_{1/2} = 0.94\Delta_{\dot{\sigma}_{max}}$ and $t_{1/2} = 0.97t_{\dot{\sigma}_{max}}$. See Section 10.6 and Ch.2 of Kao (2008) for examples of reaction zone structure with one-step models.

Sonic Singularity in Exothermic Flows

Another feature of the reaction zone that can be observed in Figs. 11.6 and 11.7 is the difference in the behavior of the Mach number as the end of the reaction zone is approached. In the case of CH_4-air, singular behavior is observed as the end of the reaction zone is approached. The rate of change of T, P, ρ and $M = w_2/a_2$ all increase without bound as $M \rightarrow 1$. This is a common feature of ZND simulations as the CJ condition computed based on the equilibrium sound speed at the end of the reaction zone is inconsistent with the Mach number based on the frozen sound approaching one as the end of the reaction zone is reached. As a consequence the quantity η defined by (9.85) may become zero before $\dot{\sigma}$ vanishes, resulting in singular behaviour with the righthand side of (9.81), (9.82), and (9.83) becoming infinite at $\eta \longrightarrow 0$.

This singular feature is not present in all steady reaction zones computations behind shock waves. In particular, this does occur in reaction zones behind *overdriven* detonations, $U > U_{\mathrm{CJ}}$; reaction zones with

Table 11.1: Characteristic reaction zone length and time scales for two examples of ZND detonation structure.

	H_2-O_2-Ar	CH_4-air	
	distance		
$\Delta_{\dot\sigma_{max}}$	9.637×10^{-4}	1.572×10^{-2}	m
$\Delta_{\dot\sigma_{0.5}}$	8.834×10^{-4}	2.579×10^{-4}	m
$\Delta_{\dot\sigma_{0.1}}$	8.753×10^{-3}	1.506×10^{-3}	m
$\Delta_{\dot\sigma_p}$	3.026×10^{-3}	7.832×10^{-4}	m
Δ_R	6.098×10^{-3}	5.2547×10^{-4}	m
	time		
$t_{\dot\sigma_{max}}$	2.422×10^{-6}	5.110×10^{-5}	s
$t_{\dot\sigma_{0.5}}$	2.065×10^{-6}	4.633×10^{-7}	s
$t_{\dot\sigma_{0.1}}$	1.680×10^{-5}	2.915×10^{-6}	s
t_p	7.360×10^{-6}	1.330×10^{-6}	s
$1/\dot\sigma_{max}$	1.54×10^{-5}	1.780×10^{-6}	s

endothermic reactions (e.g, dissociation), i.e., strong shock waves in atmospheres of planets; and detonations in many reactive mixtures with a high extent of dilution (Fig. 11.5 and 11.7). Overdriven detonations and shock waves with purely endothermic reaction zones have values of $\eta < 1$ throughout the reaction zone, i.e., the flow is always subsonic relative to the shock.

If singularities due occur when the classical CJ velocity is used for the shock speed, these usually occur near the end of the reaction zone, after the main energy release has taken place, and do not impact the computation of the characteristic length scales that are often the main objective of simulation.

One case in which the singularity appears to play an essential role is when there is a significant delayed endothermic reaction followings the main exothermic reactions. In such a case, the thermicity changes sign within the reaction zone. The classical CJ solution for the detonation speed will result in the frozen sonic point occurring within the reaction at a location where the thermicity does not vanish, resulting in singularity in the solution at that location.

In general, sonic point singularities can be resolved by considering the detonation velocity to be a free parameter $U \neq U_{\rm CJ}$ and treating the reaction zone solution as a two-point boundary-value problem. The left-hand boundary condition is determined by the postshock (frozen) state defined by U and the right-hand boundary is the sonic point at the location x^* of the frozen sonic point $\eta = 0$, where we require that

$$\dot\sigma \to 0 \text{ as } \eta = 1 - M^2 \to 0 \,, \tag{11.19}$$

such that

$$\lim_{\eta\to 0} \frac{\dot\sigma}{\eta} \text{ is finite} \,. \tag{11.20}$$

The value of U that results in the solution integrating through the point $\eta = 0$ without the solution divering is known as the *eigenvalue speed* U^*. Finding U^* requires an iterative search such as a shooting method. Fickett and Davis (1979, Ch. 5B2) refer to this the *pathological* point, and show that this point is saddle point for simplified reaction models such as two competing irreversible reactions or one reaction with a mole decrement.

For the case of a fast exothermic followed by a slower endothermic reaction, the eigenvalue speed will be higher than the classical CJ speed. Although there are a number of theoretical and numerical studies of this possibility, the only known example appears to be H_2-Cl_2 detonations Dionne et al. (2000). However, the concept of an eigenvalue solution and the reaction zone as a two-point boundary value problem arises in a number of other contexts such as quasi-steady curved detonations or detonations with distributed energy or momentum loss.

11.3 Constant volume and pressure explosions

Due the simplicity of the formulations, constant volume and constant pressure models of combustion are widely used to model a variety of ignition problems. Both models and some variations are implemented in the SDToolBox. Examples of simulations are given as demonstration programs provided in the SDToolBox.

- demo_cv_comp.py demo_cv_comp.m Generates plots and output files for a constant volume explosion simulation where the initial conditions are adiabatically-compressed reactants.
- demo_cvCJ.py demo_cvCJ.m Generates plots and output files for a constant volume explosion simulation where the initial conditions are shocked reactants using shock speed given by CJ detonation simulation.
- demo_cvshk.py demo_cvshk.m Generates plots and output files for a constant volume explosion simulation where the initial conditions are shocked reactants behind a shock traveling at a user defined shock speed U1.
- In MATLAB, the basic functions are cvsolve.m and cvsys.m; cpsolve.m and cpsys.m.
- In Python, the basic functions are cp.py and cv.py.
- demo_cv.m Generates plots and output files for constant volume explosion simulation with user specified initial conditions; uses cv_plot.m to plot temperature, pressure and species. This program estimates the effective activation energy and reaction order using the methodology described in Bane et al. (2010).
- demo_cp.m Generates plots and output files for constant pressure explosion simulation with user specified initial conditions; uses cp_plot.m to plot temperature, volume and species.

The methodology of computing effective activation energy that is implemented in these programs is described by Bane et al. (2010). Theoretical and numerical analyses have demonstrated recognized that the effective activation energy is a key parameter that is correlated with macroscopic properties such as the regularity of detonation cellular structure Austin et al. (2005). The effective activation energy can significantly vary as a function of the fuel type and mixture composition Shepherd (1986), Browne et al. (2005a).

Constant volume and constant pressure simulations are shown in Fig. 11.9 for the initial conditions (postshock or von Neumann state) of $P = 3.11$ MPa and $T = 1525$ K.

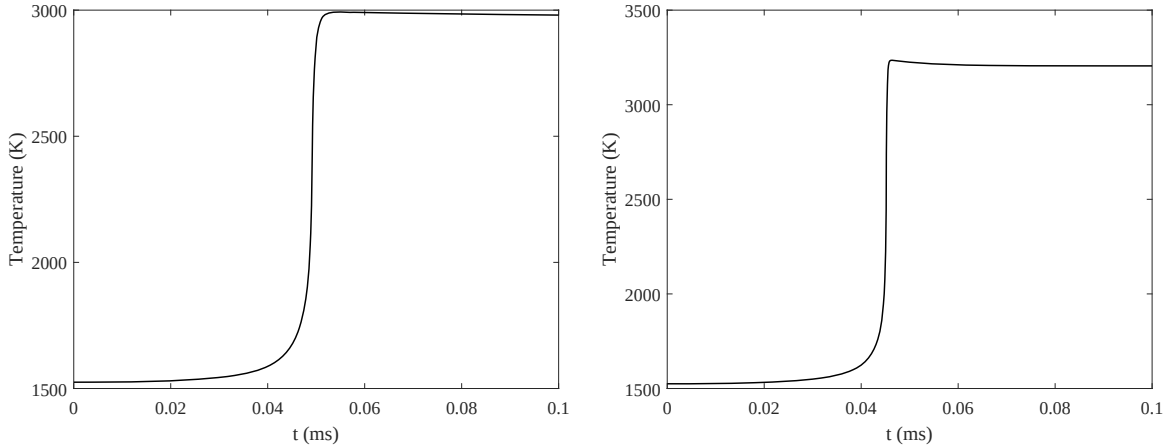

Figure 11.9: Reaction zone temporal profiles for: a) constant pressure simulation and, b) constant volume simulation with postshock conditions for CJ a detonation in a stoichiometric CH_4-air mixture.

Constant-volume simulations have been used by Westbrook and co-workers Westbrook (1982b,a)to estimate the induction time t_i based on maximum temperature rate of change and reaction zone length $\Delta_i = w_2 t_i$, where w_2 is evaluated at the von Neumann state. A comparison between the ZND model values of $\Delta_{\dot{\sigma}_{max}}$ and Δ_i is discussed by Shepherd (1986). Both the ZND and CV models have been extensively used to predict the effect of fuel type, concentration, dilution and initial temperature effects on detonation parameters through empirical correlations of reaction zone length with cell width, critical tube diameter and initiation energy. Less commonly, constant-pressure simulations are also used for this purpose. The predicted reaction zone lengths by these three models are within 10-15% (Table 11.2) and for the purposes of empirical detonation parameter correlations Westbrook and Urtiew (1982), Tieszen et al. (1991), any of the three simulations will suffice.

Model	t_i (μs)	Δ_i (mm)
ZND (thermicity peak)	50.4	15.4
CV (dT/dt_{max})	49.2	13.3
CP (dT/dt_{max})	45.2	14.5

Table 11.2: Comparison of three methods of computing reaction zone induction time and length for a stoichiometic stoichiometric CH_4-air mixture.

Constant pressure or volume computations are often used in modeling ignition delay times in shock tube experiments. An example of how the maximum rate of change of temperature with time can be used to define induction time is shown in Fig. 11.10. The temperature increase is quite modest for this highly diluted mixture but the location of the maximum in the temperature rate of change unambiguously defines the induction time.

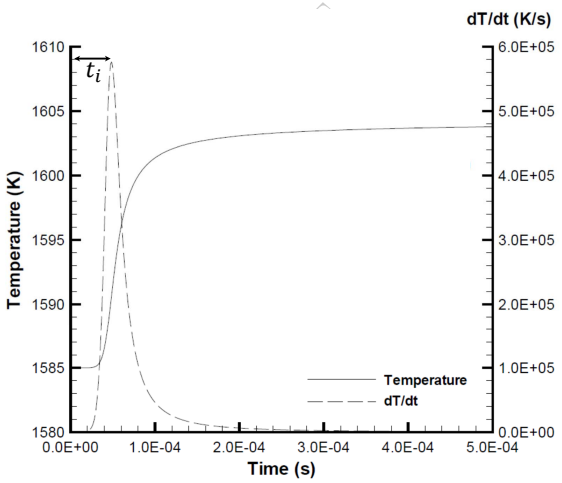

Figure 11.10: (a) Constant-volume explosion simulation of reaction behind a reflected shock wave for $0.1H_2 + 0.05O_2 + 99.85Ar$ at $P_1 = 64$ atm and $T_1 = 1585$ K. The induction time determined from the location of the peak in dT/dt is $\tau_i = 48$ μs, (Fig. 54 Schultz and Shepherd, 2000)

11.4 Unsteady Control Volume Models

The constant-pressure and constant-volume limits can be generalized to treat control volumes with heat transfer and external work by using the conservation of energy and mass. For a fixed amount of mass M, only the energy conservation equation need be considered in the form

$$\frac{dE}{dt} = \dot{W} + \dot{Q} \, . \tag{11.21}$$

If the only component of energy is the internal thermodynamic energy, we can express the left-hand side for an ideal gas as

$$\frac{\mathrm{d}E}{\mathrm{d}t} = Mc_v\frac{\mathrm{d}T}{\mathrm{d}t} + M\sum_{k=1}^{K} e_k\frac{\mathrm{d}Y_k}{\mathrm{d}t} \ , \tag{11.22}$$

and the species mass fractions can be computed from the reation mechanisms and rates as

$$\frac{\mathrm{d}Y_k}{\mathrm{d}t} = \frac{\mathcal{W}_k\dot{\omega}_k}{\rho} \ . \tag{11.23}$$

For a fluid system, the external work per unit mass is

$$\frac{\dot{W}}{M} = -P\frac{\mathrm{d}v}{\mathrm{d}t} \ , \qquad v = \frac{V}{M} \ , \tag{11.24}$$

and we define the heat transfer per unit mass as

$$\dot{q} = \frac{\dot{Q}}{M} \ . \tag{11.25}$$

The final form of the energy equation can be written

$$\frac{\mathrm{d}T}{\mathrm{d}t} = \frac{1}{c_v}\left[-\sum_{k=1}^{K} E_k\frac{\dot{\omega}_k}{\rho} - P\frac{\mathrm{d}v}{\mathrm{d}t} + \dot{q}\right] \ , \tag{11.26}$$

where we have converted the specific energy for each species to molar units

$$E_k = \mathcal{W}_k e_k \ . \tag{11.27}$$

In addition to computing the species evolution, the pressure has to be computed from the gas law, $P = RT/v$, as the temperature and volume evolve. If instead of considering the volume as a function of time, the pressure is more convenient, the energy equation equation can be more conveniently written in terms of the enthalpy $H = E + PV$, rather than the internal energy

$$\frac{\mathrm{d}T}{\mathrm{d}t} = \frac{1}{c_p}\left[-\sum_{k=1}^{K} H_k\frac{\dot{\omega}_k}{\rho} + v\frac{\mathrm{d}P}{\mathrm{d}t} + \dot{q}\right] \tag{11.28}$$

where we have converted the specific enthalpy for each species to molar units

$$H_k = \mathcal{W}_k h_k \tag{11.29}$$

for this form of the energy conservation equation, the volume will need to be evaluated as a function of pressure, temperature and mass fractions using the gas law $v = RT/P$.

These equations and extensions have found widespread use in developing engineering models of thermal ignition (Boettcher et al., 2012, Melguizo-Gavilanes et al., 2019), ignition in rapid compression machines (Goldsborough et al., 2017), reactions in the end gas of shock tubes used in chemical physics experiments (Tang and Brezinsky, 2006, Pang et al., 2009, Chaos and Dryer, 2010) and simplified models of ignition of gas bubbles and segments within piping with pressure transients (Shepherd, 2020, Coronel et al., 2020).

The critical decay concept postulates that ignition can only occur when the rate of change of the thermodynamic state is less than a critical value. The magnitude of the critical decay rate is function of the pathway to ignition and the manner in which the thermodynamic state varies during the ignition process. Demonstration programs for adiabatic compression with specified volume or pressure changes were developed for the study described in Shepherd (2020).

- demo_cdr.m Generates plots and output files for a constant volume explosion simulation with critical decay rate model using exponential increase in volume following instantaneous isentropic compression.

- demo_cdr_exp_critical.m Generates plots and output files for for a constant volume explosion simulation with critical decay rate model using exponential increase in volume following instantaneous isentropic compression. Computes critical decay rate by successive approximation.

- demo_pulse_cdr.m Computes adiabatic compression and explosion with a specified volume as a function of time. Set up for Gaussian pulse model with two parameters:CR - compression ratio (Vmax/Vmin); τ - pulse width parameter in Gaussian function. Requires two functions: `f_volume.m` - defines normalized volume and derivative as a function of time; `cvsys_v.m` to carry out the integration of energy and species equations. Integrates the equations twice, once for nonreactive, once for reactive case. Computes a single case with specified parameters. Optionally plots output for thermodynamic quantities and species.

- demo_pulse_tau_critical.m Extension of the program `demo_pulse_cdr.m` to multiple values of compression ratio and determines the critical value of τ for each.

- demo_TransientCompression.m Explosion computation simulating adiabatic compression ignition by a piston with prescribed mass and applied pressure. Requires `adiasys.m` function for ODE solver.

11.5 Reaction zones with stream tube area change

If the flow can be considered quasi-one dimensional and the stream tube cross section area $A(x)$ variation with distance is known, as in flow constrained by rigid nozzle, the mass conservation relationship is changed to

$$\rho \mathrm{w} A = \rho_1 \mathrm{w}_1 A_1 \ . \tag{11.30}$$

The energy conservation and species evolution equations are unchanged, however the momentum equation cannot in general be integrated exactly and $A(x)$ may be unknown and have to be determined as part of the flow solution. For this reason, the DAE form of the equations cannot be used for computation in the general case. Instead we take the same approach as with the detonation reaction zone and compute the structure as a solution to the equivalent set of ordinary differential equations that govern the flow behind the shock front. The differential form of the equations that can be extended to nozzles, stagnation point flow or curved shock waves is derived next.

The flow will be modeled as adiabatic, inviscid, quasi-one-dimensional and reacting. The stream tube area A has be specified as a function of distance or computed as part of solution process as discussed in the next section. Differentiating the algebraic conservation equations we obtain the conventional quasi-one-dimensional flow relations.

$$\frac{\mathrm{d}}{\mathrm{d}x}(\rho \mathrm{w}) = -\rho \mathrm{w} \frac{1}{A}\frac{\mathrm{d}A}{\mathrm{d}x} \tag{11.31}$$

$$\rho \mathrm{w} \frac{\mathrm{dw}}{\mathrm{d}x} = -\frac{\mathrm{d}P}{\mathrm{d}x} \tag{11.32}$$

$$\frac{\mathrm{d}}{\mathrm{d}x}(h + \frac{\mathrm{w}^2}{2}) = 0 \tag{11.33}$$

$$\mathrm{w}\frac{\mathrm{d}Y_k}{\mathrm{d}x} = \frac{\mathcal{W}_k \dot{\omega}_k}{\rho} \qquad (k = 1, \ldots, K) \tag{11.34}$$

11.6 Streamtube Area

There are three cases that we will consider: a) quasi-steady curved shock or detonation waves; b) stagnation point flow between a curved shock and blunt body; c) rigid nozzle flows.

Curved waves

Consider a portion of a curved shock or detonation wave with a local radius of curvature R_s, speed U and a characteristic thickness Δ. In a reference frame attached to the shock wave moving with velocity $U(t) = dR/dt$ into stationary reactants, the transformed distance and velocity variables are

$$x = R_s(t) - r \tag{11.35}$$

$$\mathrm{w} = U(t) - \mathrm{u} \tag{11.36}$$

The stream tube area change $\mathrm{d}A/\mathrm{d}x$ for slightly curved waves can be approximated (see Section 11.10 below) as

$$\alpha = \frac{1}{A}\frac{\mathrm{d}A}{\mathrm{d}x} = \kappa(\frac{D}{\mathrm{w}} - 1) \tag{11.37}$$

where κ is the curvature of the wave front

$$\kappa = \begin{cases} 2/R_s & \text{spherical waves} \\ \\ 1/R_s & \text{cylindrical waves} \end{cases} \tag{11.38}$$

This approach is valid as long as the reaction zone is thin, $R_s \gg \Delta$ and the characteristic time scale for the change in the shock speed is much longer than the passage time of fluid elements through the reaction zone, $\tau = \Delta/\mathrm{w} \ll U/(\mathrm{d}U/\mathrm{d}t)$. For positive curvature, the stream tube area $A(x)$ increases with downstream distance behind the shock front.

Stagnation point flow

For hypersonic stagnation point flow over a blunt body, numerical simulations of the complete flow field Wen and Hornung (1995), Hornung (1972), Stulov (1969) show that to a good approximation the mass flux $\rho\mathrm{w}$ decreases linearly between the shock front and body

$$\rho\mathrm{w} = \rho_\circ \mathrm{w}_\circ \left(1 - \frac{x}{\Delta}\right) \tag{11.39}$$

along the stagnation streamline, where Δ is the shock standoff distance. Treating the flow as quasi-one-dimensional on the streamtube enclosing the stagnation streamline the conservation of mass can be expressed as

$$A\rho\mathrm{w} = A_\circ \rho_\circ \mathrm{w}_\circ = \text{constant} \ . \tag{11.40}$$

From this expression and the approximate behavior of mass flux on the stagnation streamline, we compute that the logarithmic area derivative to be

$$\alpha = \frac{1}{A}\frac{\mathrm{d}A}{\mathrm{d}x} \tag{11.41}$$

$$= \frac{1}{\Delta - x} \ . \tag{11.42}$$

Although α is singular at the body, as shown below, α always enters the reaction zone equations as the product $w\alpha$ which is non-singular

$$\mathrm{w}\alpha = \frac{\mathrm{w}_\circ}{\Delta}\frac{\rho_\circ}{\rho} \tag{11.43}$$

Nozzles

For rigid nozzles, the area change $A(x)$ will be a specified function of distance

$$\alpha(x) = \frac{1}{A(x)}\frac{\mathrm{d}A(x)}{\mathrm{d}x} \tag{11.44}$$

The quasi-one-dimensional approach with specified $A(x)$ is widely used for estimates of nozzle performance as it is computationally inexpensive and reasonably reliable for mean flow properties. If knowledge of the flow uniformity is important or the nozzle is being used off-design, a more sophisticated approach will be necessary. Applications to facility design and performance usually require simulations that include viscous effects and multidimensional flow considerations.

11.7 Formulation using thermicity

A more convenient form of the reaction zone equations for numerical computation is to use elapsed time as the independent variable and to use the adiabatic change equation to eliminate the energy equation.

$$\frac{\mathrm{d}P}{\mathrm{d}t} = -\rho \mathrm{w}^2 \frac{(\dot{\sigma} - \mathrm{w}\alpha)}{\eta} \tag{11.45}$$

$$\frac{\mathrm{d}\rho}{\mathrm{d}t} = -\rho \frac{(\dot{\sigma} - \mathrm{w}M^2\alpha)}{\eta} \tag{11.46}$$

$$\frac{\mathrm{d}\mathrm{w}}{\mathrm{d}t} = \mathrm{w} \frac{(\dot{\sigma} - \mathrm{w}\alpha)}{\eta} \tag{11.47}$$

$$\frac{\mathrm{d}Y_k}{\mathrm{d}t} = \frac{\mathcal{W}_k \dot{\omega}_k}{\rho} \qquad (k = 1, \ldots, K) \tag{11.48}$$

These equations are the logical extension of the standard reaction zone model for planar waves, which is termed the ZND model in the context of detonations. The *thermicity* parameter $\dot{\sigma}$ and the sonic parameter η are as defined in Section. 9.6.

A key issue is the boundary conditions for these equations. The flow properties at the beginning of the reaction zone are those computed from the shock jump conditions evaluated at fixed composition.

$$\rho_1 \mathrm{w}_1 = \rho_\circ \mathrm{w}_\circ \tag{11.49}$$

$$P_1 + \rho_1 \mathrm{w}_1^2 = P_\circ + \rho_\circ \mathrm{w}_\circ^2 \tag{11.50}$$

$$h_1 + \frac{1}{2}\mathrm{w}_1^2 = h_\circ + \frac{1}{2}\mathrm{w}_\circ^2 \tag{11.51}$$

In these equations, states $\circ$ are the reactant conditions upstream of the shock. For a propagating shock, $\mathrm{w}_\circ = U$ - $\mathrm{u}_\circ$, where U is the shock speed and $\mathrm{u}_\circ$ is the flow speed upstream of the shock in the laboratory reference frame. For a stationary (bow) shock in the stagnation point flow situation, $\mathrm{w}_\circ$ is freestream flow velocity U in the body-fixed reference frame. State 1 is just downstream of the shock at the beginning of the reaction zone; for a detonation, this is known as the von Neumann (vN) state. In general, the jump conditions must be numerically solved for state 1.

The downstream boundary condition on the flow depends on geometry. In the case of an expanding streamtube and endothermic reactions, as in stagnation point flow, the flow will be subsonic $\eta > 0$ throughout the reaction zone and the solutions are nonsingular as long as $w\alpha$ is nonsingular. The situation is more complex for exothermic reactions, particularly detonations. For Chapman-Jouguet (CJ) waves, the flow approaches and potentially reaches the frozen sonic point, resulting in a singularity at the rear at of the reaction zone.

If the detonation is *overdriven*, $U > U_{\mathrm{CJ}}$, and α is sufficiently small, the flow will remain subsonic throughout the reaction zone and the solutions are nonsingular for all values of U. For cases where $U \leq U_{\mathrm{CJ}}$, and α is sufficiently large, there is the potential for the flow to become supersonic,, which will result in $\eta = 0$ within the reaction zone.

In those cases where the sonic parameter η passes through zero within the reaction zone, the solution will be singular unless the numerator $\dot{\sigma} - \alpha \mathrm{w}$ vanishes at the same time as η vanishes, i.e., at the sonic point $M = 1$. This is particularly important for the cases of curved quasi-steady detonation waves. Nonsingular solutions will occur only for particular values[1] of the detonation velocity D for each value of the curvature κ. The appearance of a sonic point in this flow can be attributed to the competing effects of chemical energy

[1] D is conventionally used for detonation speed U in this context

release $\dot{\sigma}$ and area change $-\mathrm{w}\alpha$ creating an effective *throat* or *converging-diverging nozzle* in the flow. The area function is actually monotonically increasing, $dA/dx > 0$, and tends to decelerate the initially subsonic flow behind the shock, driving it away from the sonic point. The thermicity $\dot{\sigma} > 0$ is positive in the main energy release region of the reaction zone and tends to accelerate the flow, driving it toward the sonic point. The appearance of a sonic point at other than a physical area minimum and the eigenvalue nature of the flow is well-known in the context of the ideal dissociating gas through a nozzle.

As a consequence of these considerations, for quasi-steady curved detonations the flow equations are a two-point boundary value problem with a regularity condition at one endpoint that will determine an eigenvalue solution $D(\kappa)$. For general reaction mechanisms and realistic thermodynamics, this problem will have to be solved numerically as a two-point boundary value problem using a method such as a shooting procedure. It is possible to obtain an analytical solution for a perfect gas with a one-step irreversible reaction described by a first-order Arrhenius rate law with a large activation energy.

The case of a converging or converging-diverging rigid nozzle also requires finding initial conditions so that the solutions are non-singular at the sonic point, $\eta = 0$. In the case of converging-diverging nozzles, the solution will be singular at an interior point and in general the location of the singularity is unknown. This requires an iterative procedure to find the physical solution that passes through the sonic point. This is an extension of the usual idea of critical mass flow rate or choking in ideal non-reacting gas dynamics.

11.8 Flows with Friction and Thermal Interactions

Reacting steady flows in ducts with friction and heat transfer can be treated using the quasi-one-dimensional formulation with empirical sources terms in the momentum and energy equations. For a steady flow in the x-direction with mean velocity u, the governing equations are most conveniently formulated in terms of the spatial derivatives.

$$\frac{\mathrm{d}}{\mathrm{d}x}(\rho \mathrm{u} A) = 0 \tag{11.52}$$

$$\rho \mathrm{u}\frac{\mathrm{du}}{\mathrm{d}x} = -\frac{\mathrm{d}P}{\mathrm{d}x} - \tilde{\tau} \tag{11.53}$$

$$\rho \mathrm{u}\frac{\mathrm{d}}{\mathrm{d}x}(h + \frac{\mathrm{u}^2}{2}) = \tilde{q} \tag{11.54}$$

$$\mathrm{u}\frac{\mathrm{d}Y_k}{\mathrm{d}x} = \frac{\mathcal{W}_k \dot{\omega}_k}{\rho} \qquad (k = 1, \ldots, K) \tag{11.55}$$

The friction force (per unit length and area of the duct) $\tilde{\tau}$ is proportional to the local wall shear stress τ_w

$$\tilde{\tau} = \frac{4}{D}\tau_w \ , \tag{11.56}$$

where $D = 4 \times$ area/perimeter is the hydraulic diameter of the duct. A common engineering approach is to define the shear stress by a skin friction coefficient c_f

$$\tau_w = \frac{1}{2}\rho \mathrm{u}^2 c_f \ , \tag{11.57}$$

or the Darcy friction factor $\Lambda = 4c_f$ given by an engineering correlation with flow Reynolds number and duct roughness.

The thermal interaction $\tilde{q}$ (per unit mass of fluid and length of the duct) can be related to the wall heat flux q_w (> 0 for transfer into the flow from the duct) and the mass flow rate

$$\tilde{q} = q_w \frac{4}{D} \ , \tag{11.58}$$